Modeling of solidification process in a rotary electromagnetic stirrer

R. Pardeshi[#], A. K. Singh[#] and P. Dutta[*]

[#] Tata Research Development and Design and Centre
54 B Hadapsar Industrial Estate, Pune 411013, INDIA

[*] Department of Mechanical Engineering
Indian Institute of Science, Bangalore 560012, INDIA

Abstract

A macroscopic model of the solidification process in a rotary electromagnetic stirrer is presented. The fluid flow, heat and mass transfer inside a rotary stirrer are modeled using 3D swirl flow equations in which turbulent flow is simulated using a k-ε model. A hybrid model is used to represent the mushy zone, which is considered to be divided into two regions: a coherent region and a non-coherent region. Each region is represented by a separate set of governing equations. An explicit time-stepping scheme is used for solving the coupled temperature and concentration fields, while an implicit scheme is used for solving equations of motion. The coupling relations also include eutectic solidification, which is an important feature in modeling solidification with electromagnetic stirring, especially in the context of the formation of semi-solid slurry. The results from the present numerical solution agree well with those corresponding to experiments reported in literature.

[*] **Corresponding author:** E-mail- pradip@mecheng.iisc.ernet.in

Nomenclature

C	Solute concentration (wt%)
c	Specific heat (J/Kg K)
D	Mass diffusivity (m^2/s)
f	Mass fraction
g	Liquid fraction
h	Enthalpy (J/Kg)
m	slope of the liquidus line
K	Thermal conductivity (W/mK)
k_0	Permeability constant
p	Pressure (Pa)
S	Source term
T	Temperature (K)
t	Time (seconds)
U	Velocity (m/s)
u	r-direction velocity component (m/s)
v_θ	θ-direction velocity component (m/s)
w	z-direction velocity component (m/s)
k	Turbulent kinetic energy
ε	Turbulent energy dissipation
Greek symbols	
α	Diffusion parameter
β	Back diffusion parameter
ρ	Density (Kg/m^3)
ρC	Mixture concentration
ρH	Mixture enthalpy
Φ	Variable
Γ	Diffusion constant
ΔH	Latent heat (J/Kg)
θ	θ - direction
Subscripts	
s	Solid
l	Liquid
eut	Eutectic
f	Fusion
old	Previous time step value
max	maximum value
t	Turbulent
r	r-direction
z	z-direction
θ	θ-direction
Superscripts	
ref	Reference value
s	solid phase

1. Introduction

Solidification of binary mixtures does not exhibit a distinct front separating solid and liquid phases. Instead, the solid is formed as a permeable, fluid saturated, crystalline-like matrix. The structure and extent of this multiphase region, known as the mushy region, depends on numerous factors, such as the boundary and initial conditions. During solidification, latent energy is released at the interfaces that separate the phases within the mushy region. The distribution of this energy therefore depends on the specific structure of the multiphase region. Latent energy released during solidification is transferred by conduction in the solid phase, as well as by the combined effects of conduction and advection in the liquid phase. Fluid motion may be induced by external means, may occur naturally by thermal and/or solutal buoyancy forces, and may also be caused by expansion or contraction of the system due to phase transformation. Concentration variations are primarily due to differences in the solubilities of constituents within each phase. Such differences lead to the selective rejection of constituents at microscopic phase interfaces. The rejected constituents are transported by fluid advection and, to a lesser extent, by diffusion within the phases.

As convection is found to be an important factor affecting solidification and transport of constituents, several researchers have made attempts to control the solidification process through fluid flow. Flow induced by magnetic fields is commonly used in the solidification processing of electrically conducting fluids such as molten metals and semiconductors [1], a practice which even dates back to the early 1930's [2]. Typically, magnetic fields may be used to promote convection deep inside the melt pool, or to suppress turbulence effects and fluctuations in melt flow. Control of melt convection has been explored in both metals and semiconductor industries, leading to improvements in both process control and product quality.

Electromagnetic stirring systems can be designed for several modes of stirring, namely rotary stirring, linear stirring, or combinations of both. Rotary stirring uses a rotating magnetic field (RMF), which is widely used in metal industries to control flow, heat and mass transfer at the solidification front [3,4] and to promote the columnar-to-equiaxed transition (CET) [4]. This effect results from swirling flow that homogenizes the liquid phase. Previous work that gave insights into the flow structure during RMF-driven solidification came from numerical [3-10] and experimental [4,9,10] research. The experimental and computational study of solidification of aluminum alloy A356 with a RMF [10] showed a significant radial and axial segregation of silicon concentration and eutectic fraction. The RMF-driven directional solidification of binary Al-7wt%Si alloy under microgravity conditions is numerically studied by Hainke et al. [8].

With strong electromagnetic stirring, dendrites can fragment at the roots, leading to the formation of semisolid slurry in the mushy region. This phenomenon has led to the development of semisolid processing of alloys [11]. The solidification process and distinct flow behavior of the semi-solid slurries during feedstock preparation needs to be understood in semisolid forming (SSF) processes. As solidification progresses, the fundamental characteristics of the stirred melt change beyond a certain critical value of solid fraction. In this context, Mat and Illegbusi [12] have developed hybrid mushy zone model to simulate flow in the mushy zone, in an attempt to predict the final macrosegregation pattern. Kumar and Dutta [13] have developed a macroscopic model for semi-solid billet casting which uses a separate solid fraction transport equation to simulate the transport of fragmented dendrites in the slurry. Recently, Chowdhury et al. [14] have developed continuum model for SSF which incorporates phenomenon of solid phase interactions.

Even though there have been several studies performed on solidification in presence of electromagnetic stirring, very little work has been reported (e.g. [10]) on models involving

eutectic fraction predictions, which is an important feature in modeling solidification involving electromagnetic stirring. A recent work on an explicit-implicit time stepping in solidification process [15] is important in the present context since, it has the flexibility to readily account for microsegregation and back-diffusion in the solid region, which can result in a more accurate prediction of eutectic solid fraction. However, it is yet to be implemented in RMF solidification problems. Also, there is no literature that uses hybrid mushy model in RMF solidification problems, which can represent semi-solid slurry more accurately. Hence in present work, a numerical model of solidification process in rotary electromagnetic stirrer that uses a partial explicit-implicit time stepping scheme [15] and a hybrid model for the mushy zone [12], is undertaken. The fluid flow, heat and mass transfer inside a rotary stirrer are modeled using 3D swirl equations where turbulent flow is modeled using a k-ε model. The mushy region is considered as completely equiaxed slurry that is divided into two regions; a mobile solid phase region and a coherent region. The hybrid mushy region model represents these two regions with separate sets of governing equations. An explicit time-stepping scheme is used for solving the coupled temperature and concentration fields, while an implicit scheme is used for solving equations of motion. Subsequently, this model is validated with experimental results reported in literature [10] for the solidification of A356 alloy in a rotary electromagnetic stirrer.

2. Mathematical model

The transport phenomena in a rotary electromagnetic stirrer are governed by the conservation of mass, momentum, energy and solute transport in 3-D swirl flow conditions. Additionally, turbulent flow is modeled through the use of two-equation k-ε model, where k is the turbulence kinetic energy and ε is the rate of dissipation of kinetic energy. The continuum mixture model, originally formulated by Bennon and Incropera [16] and later modified by

Mat and Ilegbusi [12] to include a hybrid mushy zone, is used as a starting point for modeling solidification in presence of a rotating magnetic field. In this formulation, the mushy region of equiaxed slurry is divided into two regions: (i) a non-coherent region in which solid is moving with liquid, and (ii) a coherent region in which solid does not move (i.e. u_s=0). The two mushy regions are shown schematically in figure 1. In the non-coherent mushy region where solid is moving with liquid, it is assumed that there is no relative velocity between solid and liquid phases, and that solute diffusion is negligible in comparison to transport by advection. Based on this approach, the coherent and non-coherent mushy regions are modelled using separate sets of governing equations. In the formulation of the model, the following additional assumptions are invoked:

(1) The flow is described by the conservation equations for an incompressible Newtonian fluid with constant properties,

(2) Solidification shrinkage is neglected because forced convection dominates shrinkage driven flow.

(3) The fluid velocity is substantially lower than the characteristic velocity for the driving magnetic field (low magnetic Reynold's number regime).

(4) The various material properties, including thermal conductivities, electrical conductivities, specific heats, and magnetic permeabilities are same and constant in solid as well as in liquid phases.

The macroscopic conservation equations for heat and solute are constructed according to a mixture model, by adding the equations of the two phases. To begin with, we define the solid and liquid phase enthalpies as:

$$h_s = c_s T, \tag{1}$$

$$h_l = c_l T + \Delta H, \tag{2}$$

where c_s and c_l are the solid and liquid specific heats (assumed constant in respective phases), respectively. With the above definitions, the mixture enthalpy can be expressed as:

$$[\rho H] = g_s \rho_s h_s + (1 - g_s)\rho_l h_l \tag{3}$$

Accordingly, the mixture concentration can be expressed as:

$$[\rho C] = g_s \rho_s \langle C_s \rangle^s + (1 - g_s)\rho_l C_l \tag{4}$$

Effects of turbulence are represented by the two-equation (k-ε) model using the constants reported in Launder and Spalding [17]. For unsteady and incompressible fluid flow calculations, the conservation equations for all transport variables in cylindrical co-ordinates, with swirl in θ - direction, can now be written. First, the continuity equation, which is common for both zones, is written as follows:

$$\rho\left(\frac{\partial u}{\partial r} + \frac{u}{r} + \frac{\partial w}{\partial z}\right) = 0 \tag{5}$$

For the transport of momentum, energy and solute, separate sets of governing equations are written for each zone in the mushy region. It is assumed that coherent mush exists for liquid fraction $g_l < g_c$, where g_c is a critical liquid fraction value (also called the coherency point), beyond which the mushy region is assumed to be non-coherent. The value of g_c will changes depending on morphology but we have chosen constant value (g_c = 0.6) because the solid grains are globular and uniform in a typical semisolid slurry. For the coherent zone, solid velocity is zero and the mushy region behaves like a porous medium. Hence, the equations for the coherent zone are similar to those for columnar solidification, for which the solid velocity, u_s, is zero. These equations can be written as:

r-direction momentum

$$\rho\left(\frac{\partial u}{\partial t} + u\frac{\partial u}{\partial r} + w\frac{\partial u}{\partial z} - \frac{v_\theta^2}{r}\right) = -\frac{\partial p}{\partial r} + (\mu + \mu_t)\left(\frac{\partial^2 u}{\partial r^2} + \frac{\partial}{\partial r}\left(\frac{u}{r}\right) + \frac{\partial^2 u}{\partial z^2}\right) + S_r \tag{6}$$

z-direction momentum

$$\rho\left(\frac{\partial w}{\partial t} + u\frac{\partial w}{\partial r} + w\frac{\partial w}{\partial z}\right) = -\frac{\partial p}{\partial z} + (\mu + \mu_t)\left(\frac{\partial^2 w}{\partial r^2} + \frac{1}{r}\frac{\partial w}{\partial r} + \frac{\partial^2 w}{\partial z^2}\right) + S_z \tag{7}$$

θ-direction momentum

$$\rho\left(\frac{\partial v_\theta}{\partial t}+u\frac{\partial v_\theta}{\partial r}+w\frac{\partial v_\theta}{\partial z}+\frac{uv_\theta}{r}\right)=(\mu+\mu_t)\left(\frac{\partial^2 v_\theta}{\partial r^2}+\frac{\partial^2 v_\theta}{\partial z^2}-\frac{v_\theta}{r^2}\right)+F_\theta+S_\theta \tag{8}$$

Turbulent kinetic energy equation

$$\rho\left(\frac{\partial k}{\partial t}+u\frac{\partial k}{\partial r}+w\frac{\partial k}{\partial z}\right)=\left(\mu+\frac{\mu_t}{\sigma_k}\right)\left(\frac{\partial^2 k}{\partial r^2}+\frac{1}{r}\frac{\partial k}{\partial r}+\frac{\partial^2 k}{\partial z^2}\right)+S_k \tag{9}$$

Energy dissipation equation

$$\rho\left(\frac{\partial \varepsilon}{\partial t}+u\frac{\partial \varepsilon}{\partial r}+w\frac{\partial \varepsilon}{\partial z}\right)=\left(\mu+\frac{\mu_t}{\sigma_k}\right)\left(\frac{\partial^2 \varepsilon}{\partial r^2}+\frac{1}{r}\frac{\partial \varepsilon}{\partial r}+\frac{\partial^2 \varepsilon}{\partial z^2}\right)+S_\varepsilon \tag{10}$$

Energy equation

$$\frac{\partial[\rho H]}{\partial t}+\rho C_p u\frac{\partial T}{\partial r}+\rho C_p w\frac{\partial T}{\partial z}=K\left(\frac{\partial^2 T}{\partial r^2}+\frac{1}{r}\frac{\partial T}{\partial r}+\frac{\partial^2 T}{\partial z^2}\right) \tag{11}$$

Solute Transport

$$\frac{\partial[\rho C]}{\partial t}+\rho u\frac{\partial C_l}{\partial r}+\rho w\frac{\partial C_l}{\partial z}=0 \tag{12}$$

The non-coherent zone ($g_l > g_c$) is characterized by solid particles moving with the liquid without any relative velocity (i.e. $u_s = u_l$) and drag between solid-liquid phases is neglected. The corresponding the governing equations are as follows:

r-direction momentum

$$\rho\left(\frac{\partial u}{\partial t}+u\frac{\partial u}{\partial r}+w\frac{\partial u}{\partial z}-\frac{v_\theta^2}{r}\right)=-\frac{\partial p}{\partial r}+(\mu_0+\mu_t)\left(\frac{\partial^2 u}{\partial r^2}+\frac{\partial}{\partial r}\left(\frac{u}{r}\right)+\frac{\partial^2 u}{\partial z^2}\right) \tag{13}$$

z-direction momentum

$$\rho\left(\frac{\partial w}{\partial t}+u\frac{\partial w}{\partial r}+w\frac{\partial w}{\partial z}\right)=-\frac{\partial p}{\partial z}+(\mu_0+\mu_t)\left(\frac{\partial^2 w}{\partial r^2}+\frac{1}{r}\frac{\partial w}{\partial r}+\frac{\partial^2 w}{\partial z^2}\right) \tag{14}$$

θ-direction momentum

$$\rho\left(\frac{\partial v_\theta}{\partial t}+u\frac{\partial v_\theta}{\partial r}+w\frac{\partial v_\theta}{\partial z}+\frac{uv_\theta}{r}\right)=(\mu_0+\mu_t)\left(\frac{\partial^2 v_\theta}{\partial r^2}+\frac{\partial^2 v_\theta}{\partial z^2}-\frac{v_\theta}{r^2}\right)+F_\theta \tag{15}$$

Turbulent kinetic energy equation

$$\rho\left(\frac{\partial k}{\partial t}+u\frac{\partial k}{\partial r}+w\frac{\partial k}{\partial z}\right)=\left(\mu_0+\frac{\mu_t}{\sigma_k}\right)\left(\frac{\partial^2 k}{\partial r^2}+\frac{1}{r}\frac{\partial k}{\partial r}+\frac{\partial^2 k}{\partial z^2}\right)+S_k \tag{16}$$

Turbulent energy dissipation equation

$$\rho\left(\frac{\partial \varepsilon}{\partial t}+u\frac{\partial \varepsilon}{\partial r}+w\frac{\partial \varepsilon}{\partial z}\right)=\left(\mu_0+\frac{\mu_t}{\sigma_k}\right)\left(\frac{\partial^2 \varepsilon}{\partial r^2}+\frac{1}{r}\frac{\partial \varepsilon}{\partial r}+\frac{\partial^2 \varepsilon}{\partial z^2}\right)+S_\varepsilon \tag{17}$$

Energy equation

$$\frac{\partial[\rho H]}{\partial t}+\rho C_p u\frac{\partial T}{\partial r}+\rho C_p w\frac{\partial T}{\partial z}=K\left(\frac{\partial^2 T}{\partial r^2}+\frac{1}{r}\frac{\partial T}{\partial r}+\frac{\partial^2 T}{\partial z^2}\right)-\rho u\frac{\partial \Delta H}{\partial r}-\rho w\frac{\partial \Delta H}{\partial z} \tag{18}$$

Solute Transport

$$\frac{\partial[\rho C]}{\partial t}+u\frac{\partial[\rho C]}{\partial r}+w\frac{\partial[\rho C]}{\partial z}=0 \tag{19}$$

The constants used in the equations for k and ε are [17],

$$\sigma_k=1.0,\ \sigma_\varepsilon=1.3,\ c_{\varepsilon 1}=1.44 \text{ and } c_{\varepsilon 2}=1.92. \tag{20}$$

The differences in source terms pertaining to energy equations for coherent and non-coherent zones arise due to the presence of mush convection in the latter case. Some of the other source terms used in the above equations are as follows:

$$F_\phi=\frac{1}{2}\sigma B_0^2\omega r\exp\left(\frac{-2\left(z-z_{mid}\right)^2}{z_{width}^2}\right)\left(1-\frac{v_\theta}{\omega r}\right)\hat{\theta} \tag{21}$$

$$S_k=\mu_t\left(\frac{\partial u_i}{\partial x_k}+\frac{\partial u_k}{\partial x_j}\right)\frac{\partial u_i}{\partial x_k}-\rho\varepsilon \tag{22}$$

$$S_\varepsilon=\frac{\varepsilon}{k}c_{\varepsilon 1}\mu_t\left(\frac{\partial u_i}{\partial x_k}+\frac{\partial u_k}{\partial x_j}\right)\frac{\partial u_i}{\partial x_k}-c_{\varepsilon 2}\rho\frac{\varepsilon}{k} \tag{23}$$

The convective term of mixture solute equations is given by following equation,

$$[\rho Cu]=g_s\rho_s\left\langle C_s\right\rangle^s u_s+(1-g_s)\rho_l C_l u_l \tag{24}$$

For the coherent zone, $u_s = 0$, hence the above equation will be modified as:

$$[\rho Cu]=(1-g_s)\rho_l C_l u_l \tag{25}$$

For the non-coherent zone, $u_s = u_l$, hence the equation will be modified as:

$$[\rho Cu]=\left(g_s\rho_s\left\langle C_s\right\rangle^s+(1-g_s)\rho_l C_l\right)u_l=[\rho C]u \tag{26}$$

From fluid flow perspective, the main difference in coherent and non-coherent region is in way we model the mushy region, wherein the solid phase velocity is zero in the coherent region and it is equal to liquid phase velocity in the non-coherent mushy region. The additional source terms in momentum equations for the coherent zone come from the Carman-Kozeny model for flow through porous mushy region. The Carman-Kozeny relations are represented as [19]:

$$S_r = k_0 \frac{g_s^2}{(1-g_s)^3} u,\ S_\theta = k_0 \frac{g_s^2}{(1-g_s)^3} v_\theta,\ S_z = k_0 \frac{g_s^2}{(1-g_s)^3} w \tag{27}$$

In the non-coherent mushy region, the slurry molecular viscosity variation with solid fraction, as given in ref [18], has been used:

$$\mu_0 = \mu \exp(4.5 g_s) \qquad for\ g_l \geq g_c \tag{28}$$

3. Numerical Details

In the present study, a non-uniform structured grid is used as shown in figure 2. Initially, [ρH] and [ρC] are solved using the explicit scheme. Subsequently, coupling equations are solved, undergoing inner iterations. In the present study, the temperature – concentration coupling used is similar to that described in Voller et al. [19]. A full description of the explicit form of equations for solute and temperature and the explicit-implicit algorithm is given in Pardeshi et al. [15]. The momentum equations, along with the continuity equation, are discretized using a finite volume method (FVM) as described in Patankar [20]. These equations are discretized using implicit time stepping scheme. The momentum and continuity equations are solved using the SIMPLER algorithm [20] and tri-diagonal matrix solver. Convergence is declared in the implicit iteration loop when $|(\phi-\phi_{old}) / \phi_{max}| < 10^{-5}$, where ϕ stands for solved variables at a grid point at the current iteration level, ϕ_{old} represents the corresponding value at the previous iteration level, and ϕ_{max} is the maximum value of the variable at the current iteration

level in the entire domain. The convergence criterion for the iterative loop that solves the coupling equations is that the correction in the nodal solid fraction value satisfies the condition $|g-g_{old}| < 10^{-4}$, where g is solid fraction value at current iteration and g_{old} is solid fraction value at previous iteration.

4. Results and Discussion

The numerical model developed here is applied for the case of solidification of Al-7 wt %Si alloy in a rotary electromagnetic stirrer. The test case corresponds to an experimental study reported in literature [10], in which Al-7wt %Si (A356) alloy is solidified in a bottom-cooled cylindrical cavity. The side wall of the cavity is insulated. For the present simulations, the bottom surface heat transfer coefficient is obtained from experimental temperature measurements [10]. A zero mass flux condition prevails on all the walls of the cavity for the solute conservation equation. The binary fluid is considered to be Newtonian and incompressible, and its thermo-physical data are given in Table 1. A non-uniform grid system of 30×80 grids and a time step of 0.0001 seconds are used for the simulations.

After 5 seconds of cooling at the bottom wall, current to the magnetic coil is switched on, creating a rotating electro-magnetic field in the cavity. The force field is generated using a current supply of 12 amperes. The electromagnetic force distribution used in the present simulation is the same as that used in [10]. With the given condition, solidification of the alloy commences immediately at the cold bottom boundary. At later times, three regions will exist in the cavity: a fully solid region, a mushy region, and a fully liquid region. Some pertinent results from the simulations are discussed below.

4.1 Evolution of flow pattern

In present mathematical model, the driving force (Lorentz force) for fluid flow is in the swirl direction (i.e. in θ - direction), which leads to primary flow in that direction. Figure 3 (a)

shows the flow field in the θ-direction, which has variation in radial as well as in axial directions. Figure 3 (b) shows a contour plot of the θ-direction velocity component. This primary flow gives rise to a secondary flow in the r-z plane. The secondary flow in radial and axial directions is due to pressure field evolutes from the primary flow. Figure 4 shows streamlines due to secondary flow at three different time levels (at 10, 40, and 80 seconds) after start of solidification. As shown in fig. 4, the secondary flow has two cells originating as a result of variation of magnetic field in the z-direction, which agrees well with previous findings reported in literature [10]. The cell at the bottom has anti-clockwise motion while the top cell has flow in the clockwise direction. With progress in solidification, the bottom cell decreases in size, as observed from the streamline patterns at later times.

4.2 Progress of Solidification

Figure 5 shows progress of solidification at the same time levels (at 10, 40, and 80 seconds). In the non-coherent mushy region, where the solid phase is mobile, there is evidence of solid phase transport from the bottom to the top of the cavity, due to the action of the secondary convection cells. On the other hand, the coherent mushy region with stationary solid is a thinner region. Because of the anti-clockwise nature of flow in the bottom cell, the mushy region gets deformed into a dome-like shape.

4.3 Solute Transport

The solute transport, and hence macrosegregation patterns, are also expected to be different in the two zones of the mushy region. Figure 6 (a) and 6(b) shows contours of liquid concentration (at 10, and 40 seconds), which shows solute transport from the bottom to the top of the cavity in the central region. In the coherent mushy region, macrosegregation occurs as the rejected solute in this region is transported from the bottom of the cavity to the top due to fluid flow. In the non-coherent zone, however, the solid phase moves with same velocity as the liquid phase, and this does not lead to any macrosegregation. Figure 6 (c) shows the

macrosegregation pattern, which shows negative segregation at the bottom and positive segregation at the top of the cavity.

4.4 Comparison of eutectic solid fraction with experimental data

Figure 7 shows eutectic solid fraction variation in the axial direction along the central axis from the bottom of the cavity to the top, and the prediction from the model is compared with experimental and simulation results given in [10]. It is observed in fig. 7 that the eutectic fraction dips in the region close to the bottom surface, rises again and stays at a nearly constant level up to the top of the cavity. This axial variation of eutectic concentration mimics the interfacial solute concentration variation with time, as the interface progresses from the bottom to the top. The initial solidification forms a solute-rich liquid layer at the interface, leading to high eutectic concentration in the solid. However, after the stirrer is switched on at time t = 5 seconds, there is a sudden drop in concentration due to transport of solute from the bottom of the cavity to the top. Due to solute transport, this solute-depleted region will solidify mostly in a non-eutectic manner. Thereafter, vigorous fluid flow promotes motion of solid phase and good mixing of solute, the producing a homogeneous slurry. This slurry progressively solidifies with a nearly constant eutectic solid fraction. Figure 8 shows variation of eutectic fraction in the radial direction. The trend predicted by the present model shows a good agreement with experimental data.

Effect of back diffusion parameter

Microsegregation models are useful components in large-scale simulations of alloy solidification systems in predicting the final concentration distribution. In this context, an important role of a microsegregation model is to provide an estimate of the dilution (assuming a partition coefficient of less than unity) of the liquid phase due to the back-diffusion into the solid. In binary eutectic alloys, the dilution will affect the amount of eutectic phase that forms. In the present simulation, the explicit-implicit scheme [15] uses a dynamic back-diffusion

model to make a quantitative assessment of the effect of back diffusion on the prediction of eutectic fraction. Comparison of two extreme cases of no back-diffusion $\beta=0$ and complete solid state diffusion $\beta=1$ is shown in figure 9. The eutectic fraction profile at the end of solidification is shown along the axis of the cylindrical casting. In the case of no (or low) back-diffusion, the dilution of liquid concentration is negligible, and hence the amount of eutectic formation is larger than that formed with a large back-diffusion parameter.

6. Conclusions

A numerical model of solidification process in rotary electromagnetic stirrer is presented. The fluid flow, heat and mass transfer inside a rotary stirrer are modeled using 3D swirl flow equations where turbulent flow is modeled using a k-ε turbulence model. The explicit approach results in a local point-by-point coupling scheme for the temperature and concentration fields that uses constitutive model for back diffusion in solid. The coupling equations also accounts for eutectic solidification, which is an important parameter in production of semisolid casting using electromagnetic stirring. Results from the present model show a good agreement with experimental data on eutectic fraction prediction and marginal improvement over results from existing simulations. The eutectic fraction distribution at a later stage of solidification shows a nearly uniform pattern, suggesting good mixing due to stirring. Inclusion of back diffusion effects in the model results in significant difference in prediction of final eutectic fraction.

References

1. P.A. Davidson, An Introduction to Magnetohydrodynamics, Cambridge University Press, Cambridge, 2001

2. A.A. Tsavaras, H.D. Brody, Electromagnetic stirring and continuous casting-achievements, problems and goals, J. Met. 167 (1984) 31–37.
3. B. Willers, S. Eckert, U. Michel, G. Zouhar, Effect of the fluid convection driven by a rotating magnetic field on the solidification of a PbSn alloy, in: D.M. Herlach (Ed.), Solidification and Crystallization, Wiley-VCH Verlag GmbH & Co. KGaA, Weinheim, 2004.
4. B. Willers, S. Eckert, U. Michel, I. Haase, G. Zouhar, The columnar to equiaxed transition in Pb–Sn alloys affected by electromagnetically driven convection, Mater. Sci. Eng. A 402 (2005) 55–65.
5. P.A. Nikrityuk, M. Ungarish, K. Eckert, R. Grundmann, Spin-up of a liquid metal flow driven by a rotating magnetic field in a finite cylinder. A numerical and analytical study, Phys. Fluids 17 (2005),067101.
6. P.A. Nikrityuk, K. Eckert, R. Grundmann, Numerical study of spinup dynamics of a liquid metal stirred by rotating magnetic fields in a cylinder with the upper free surface, Magnetohydrodyn. J. 40 (2004) 127–146.
7. Th. Kaiser, K.W. Benz, Taylor vortex instabilities induced by a rotating magnetic field: a numerical approach, Phys. Fluids 10 (5)(1998) 1104–1110.
8. M. Hainke, J. Friedrich, G. Müller, Numerical study on directional solidification of AlSi alloys with rotating magnetic fields under microgravity conditions, J. Mater. Sci. 39 (2004) 2011–2015.
9. S. Eckert, B. Willers, G. Gerbeth, Measurements of the bulk velocity during solidification of metallic alloys, Metall. Mater. Trans. A 36A (2004) 267–270.
10. J. K. Roplekar, J. A. Dantzig. A study of solidification with a rotating magnetic field. Int. J. Cast Metals Research, vol. 14 (2001), pp. 79–98.
11. Spencer D. R., Flemings M. C., Rheocasting, Mater. Sci. Eng, 25 (1976) 103- 107.

12. M. D. Mat, O. J. Ilegbusi, Application of a hybrid model of mushy zone to macrosegregation in alloy solidification, Int. J. Heat Mass Transfer, vol. 45 (2002), 279-289.
13. Kumar and P. Dutta, Modeling of transport phenomena in continuous casting of non-dendritic billets, Int. J. Heat Mass Transfer, 48 (2005) , 3674–3688.
14. J. Chowdhury, S. Ganguly, S. Chakraborty, Implication of solid phase interaction mechanisms on momentum, heat and solute transport in semi-solid material processing, Int. J. Heat Mass Transfer, 50 (2007), 2692-2703.
15. R. Pardeshi, V. R. Voller, A. K. Singh and P. Dutta, An explicit-implicit time stepping scheme for solidification models, Int. J. Heat Mass Transfer, *in press* (2008).
16. W. D. Bennon and F. P. Incropera, A continuum model for momentum, heat and species transport in binary solid-liquid phase change systems- I. Model formulation, Int. J. Heat Mass Transfer, vol. 30, No. 10 (1987), 2161-2170.
17. B. Launder and D. Spalding, The numerical computation of turbulent flows, Comp. Meth. in Appl. Mech. Eng., **3** (1974), 269.
18. Y. Ito, M. C. Flemings, and J. A. Cornie, Rheological behavior and microstructure of Al-6.5wt%Si alloy, in Nature and Properties of Semi-solid Materials (J. A. Sekhar and J. A.Dantzig, eds.), (San Diego, CA), pp. 3–17, 1992.
19. V. R. Voller, Chapter 19: Numerical methods for phase-change problems, Handbook of Numerical Heat Transfer, 2nd Edition, W. J. Minkowycz, E. M. Sparrow and J. Y. Murthy (2006).
20. S. V. Patankar, Numerical Heat Transfer and Fluid Flow. Hemisphere, Washington, DC (1980).

List of figures

Figure 1 : Schematic of mushy region

Figure 2 : Non-uniform mesh distribution and boundary conditions

Figure 3 : flow field in θ - direction at time = 8 seconds (a) 3 dimensional velocity vectors at several sections in z- direction (b) contour plot of θ - direction velocity component

Figure 4 : Streamlines plot at different time levels (a)10 seconds, (b) 40 seconds and (c) 80 seconds after start of solidification

Figure 5 : Liquid fraction contours at different time levels (a)10 seconds, (b) 40 seconds and (c) 80 seconds after start of solidification

Figure 6 : Solute concentration contours (a) liquid concentration profile at time = 10 seconds after (b) liquid concentration profile at time = 40 seconds (c) Final macrosegregation profile

Figure 7 : Eutectic solid fraction variation along z-direction

Figure 8 : Eutectic solid fraction variation along r-direction

Figure 9 : Effect of back diffusion parameter

List of tables

Table 1 : Thermo-physical properties of Al – 7 wt% Si

Table 1 : Thermo-physical properties of Al – 7 wt% Si

Property	Value
Partition coefficient (k)	0.13
Eutectic composition (Ce)	12.6 % Si
Liquidus slope	-6.9047 °C / %Si
Melting temperature of pure aluminum	660 °C
Specific heat	963 J/Kg K
Latent heat	397500 J/Kg
Molecular viscosity of liquid	10^{-2} Pa.s
Electrical conductivity	4.0×10^{6} 1/Ωm

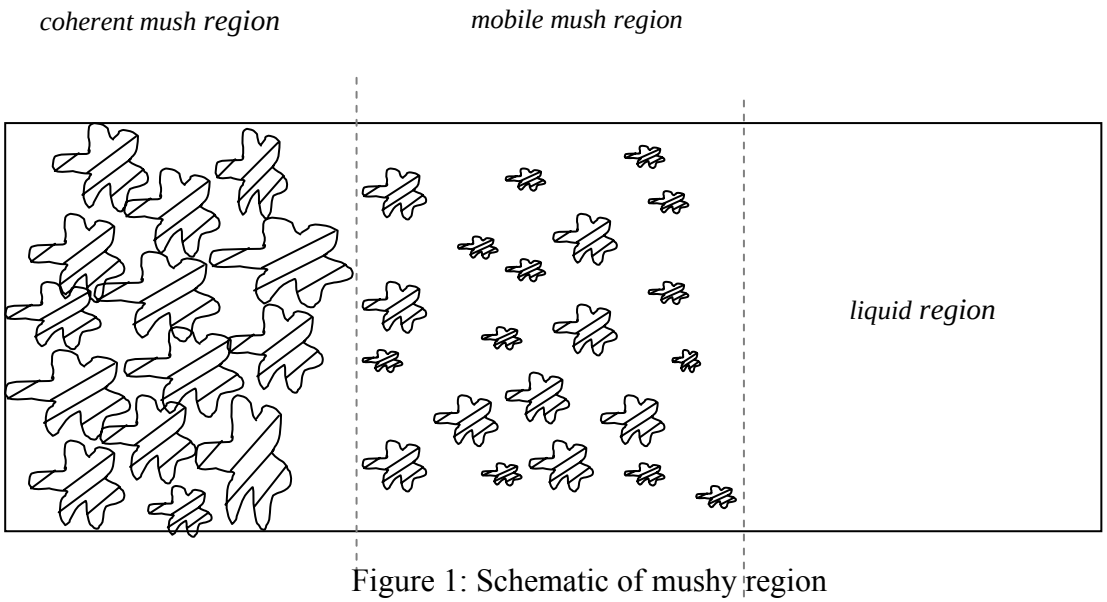

Figure 1: Schematic of mushy region

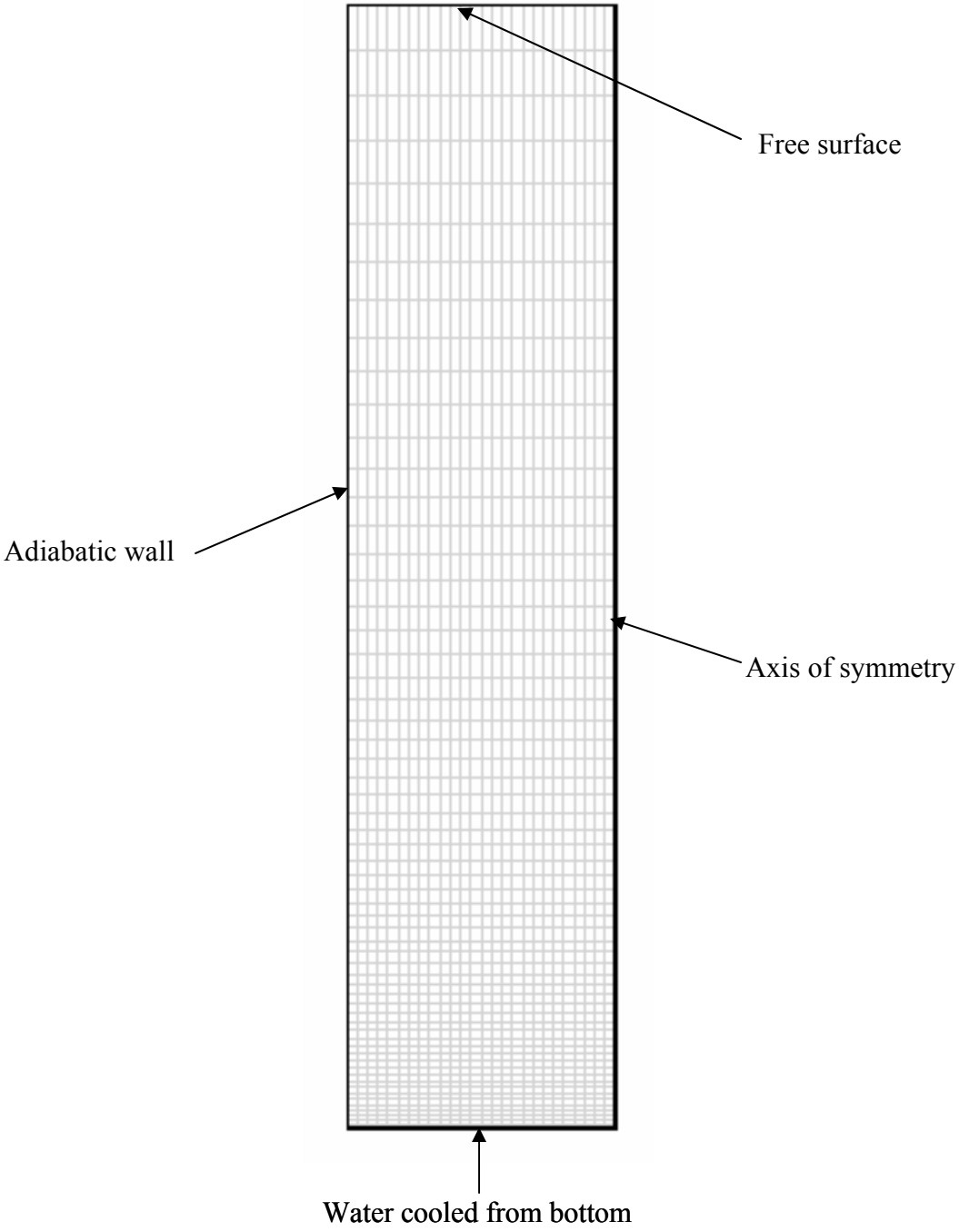

Figure 2 : Non-uniform mesh distribution and boundary conditions

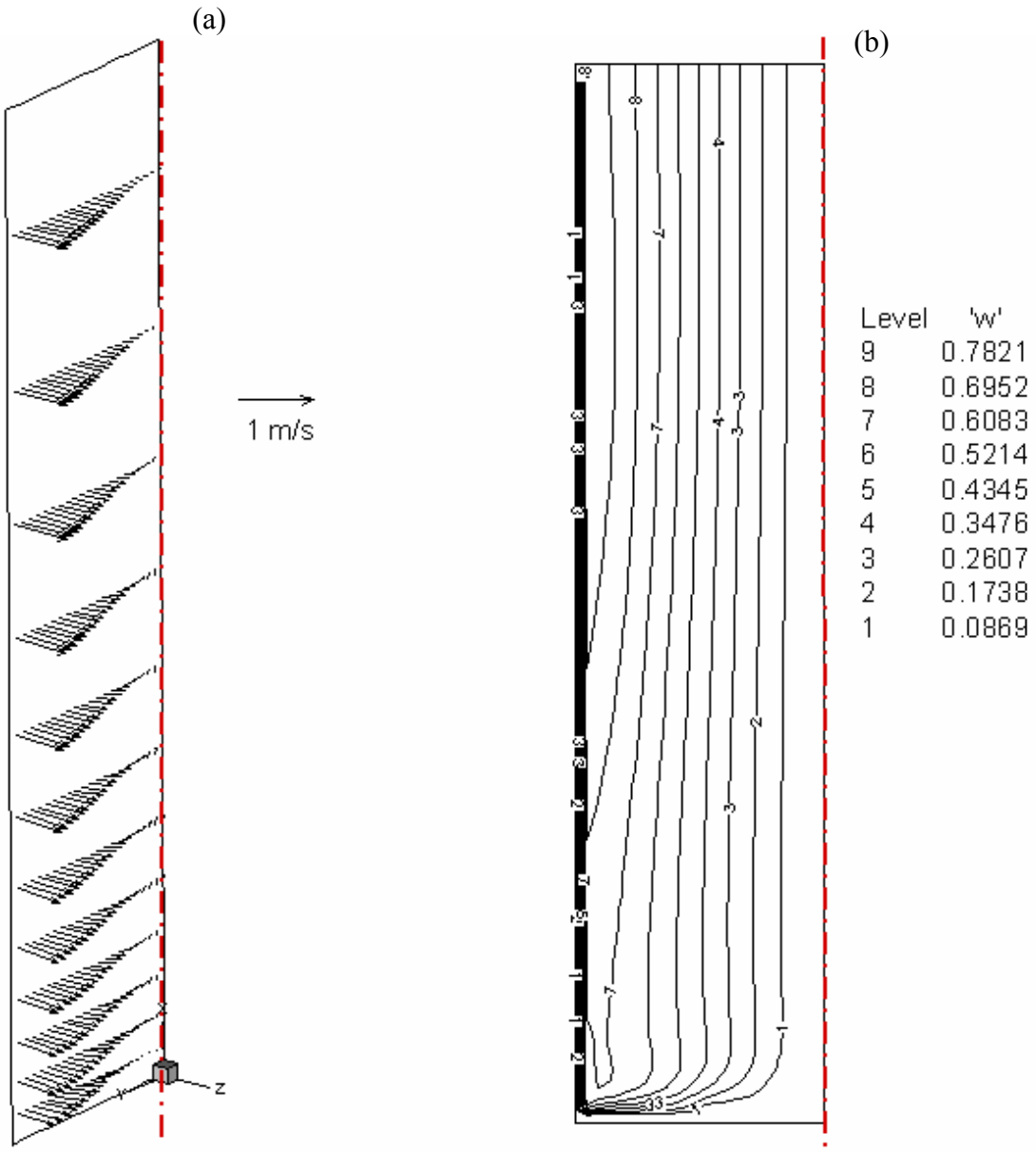

Figure 3 : flow field in θ - direction at time = 8 seconds (a) 3 dimensional velocity vectors at several sections in z- direction (b) contour plot of θ - direction velocity component

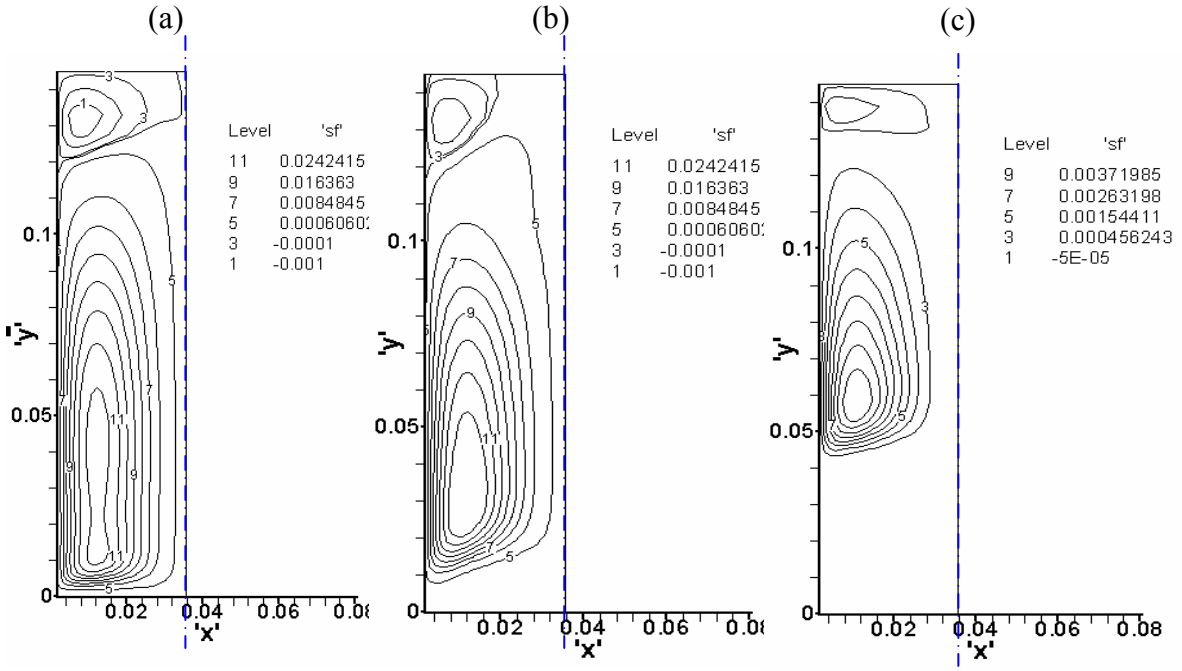

Figure 4 : Streamlines plot at different time levels (a)10 seconds, (b) 40 seconds and (c) 80 seconds after start of solidification

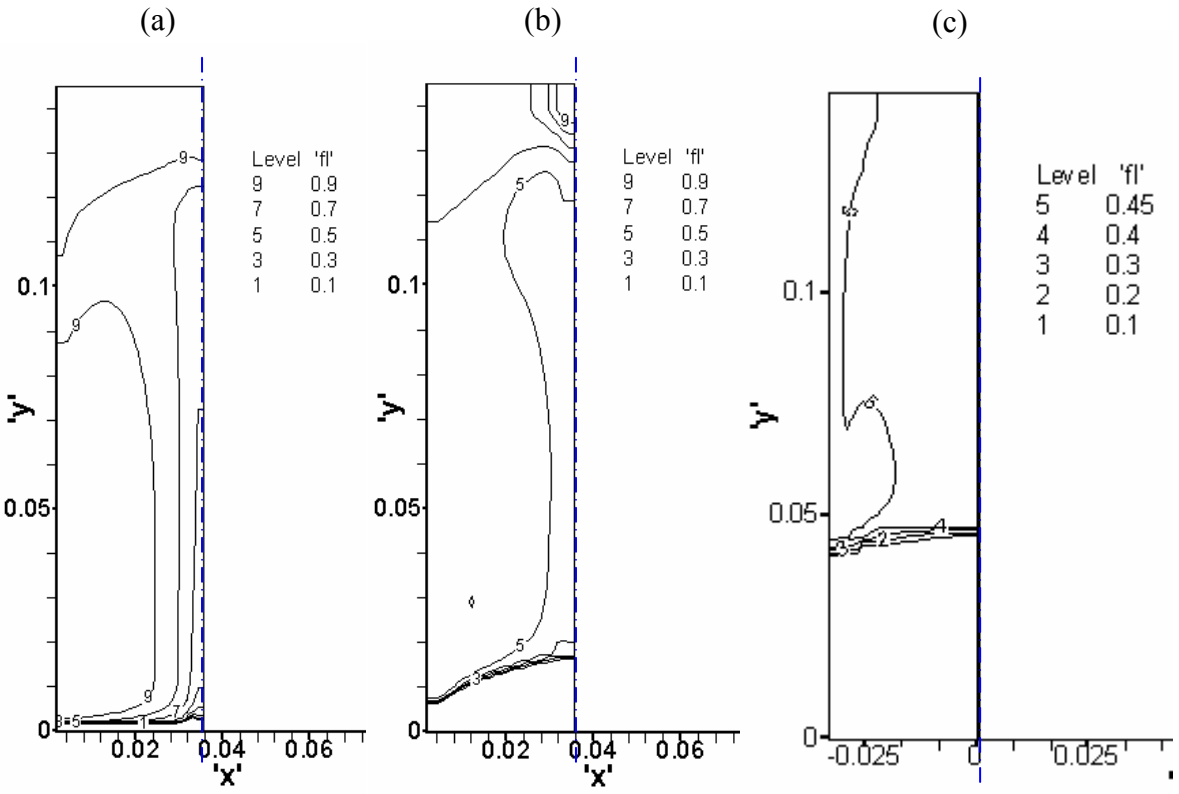

Figure 5 : Liquid fraction contours at different time levels (a)10 seconds, (b) 40 seconds and (c) 80 seconds after start of solidification

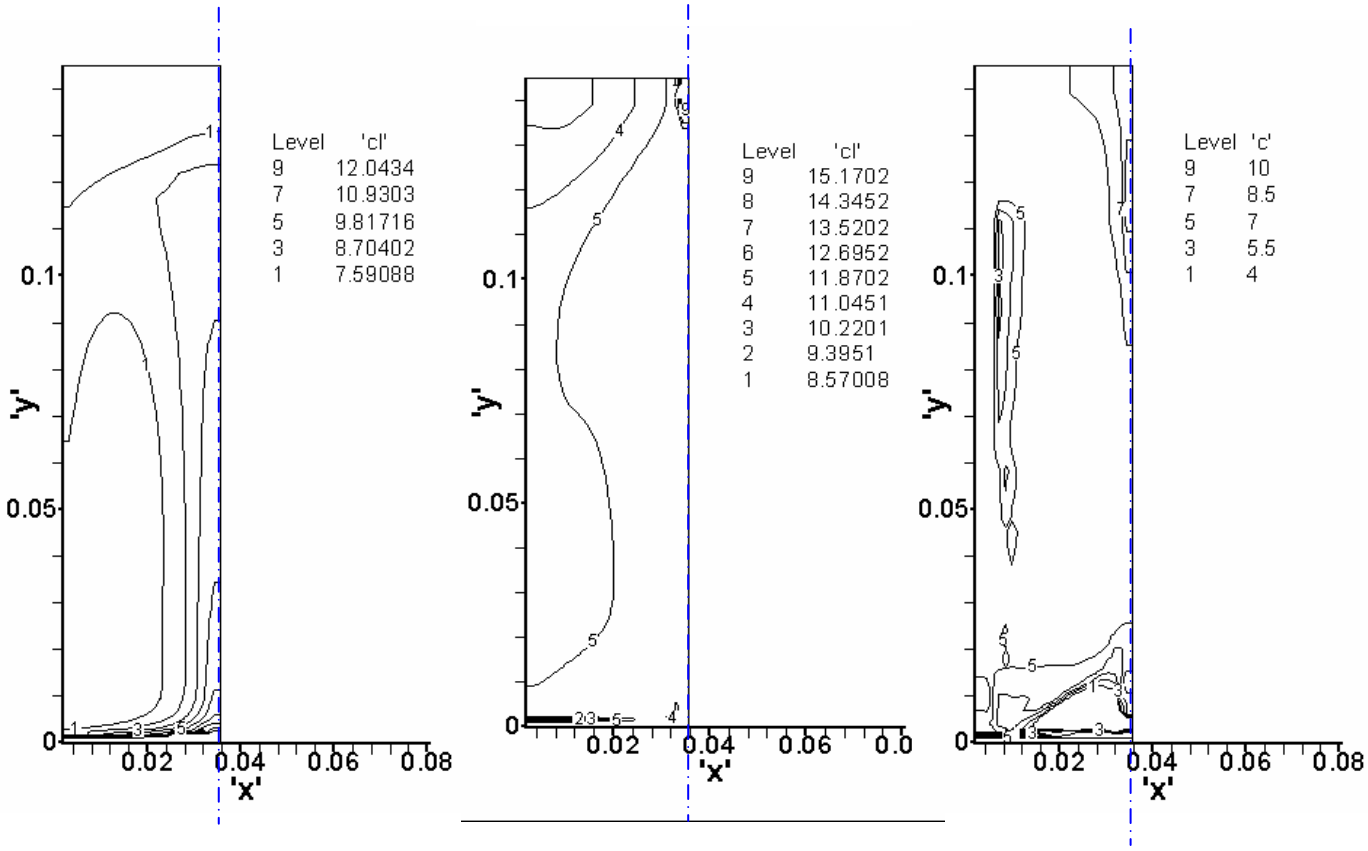

Figure 6 : Solute concentration contours (a) liquid concentration profile at time = 10 seconds after (b) liquid concentration profile at time = 40 seconds (c) Final macrosegregation profile

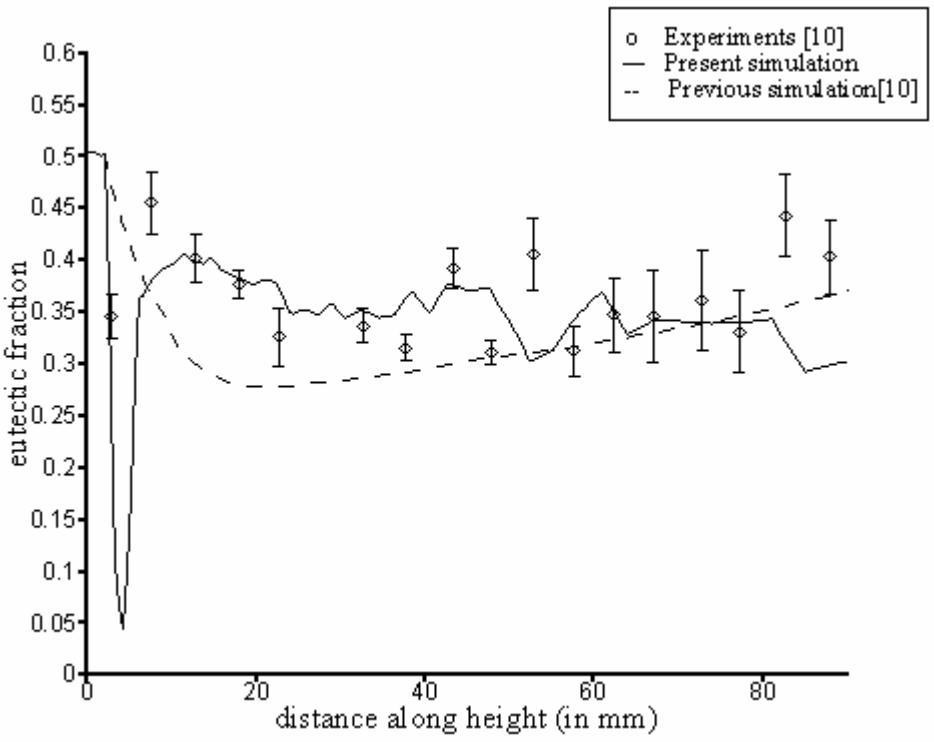

Figure 7 : Eutectic solid fraction variation along z-direction

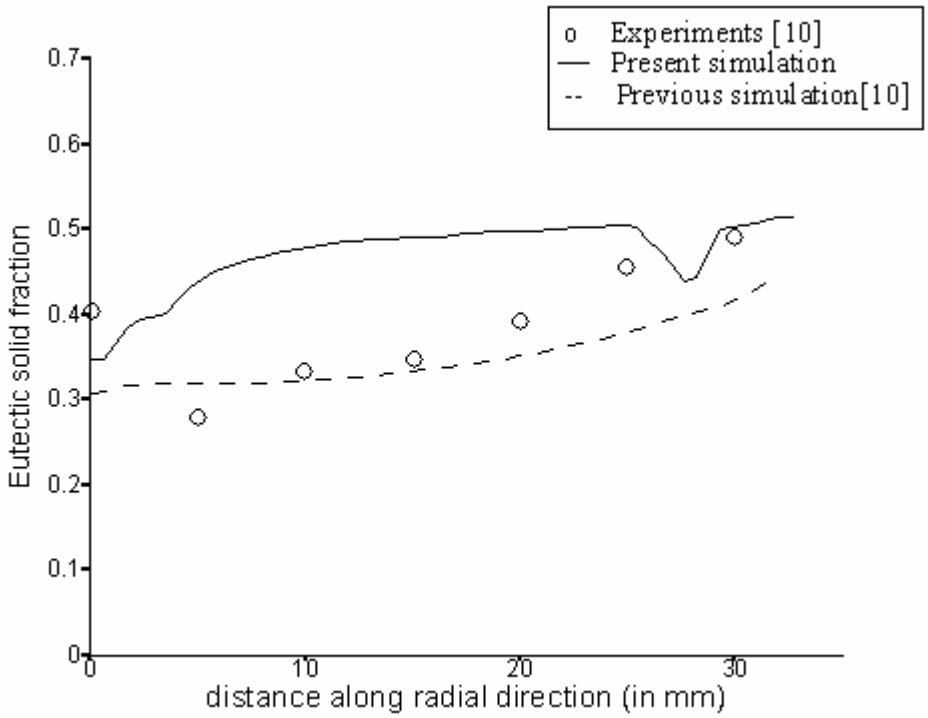

Figure 8 : Eutectic solid fraction variation along r-direction

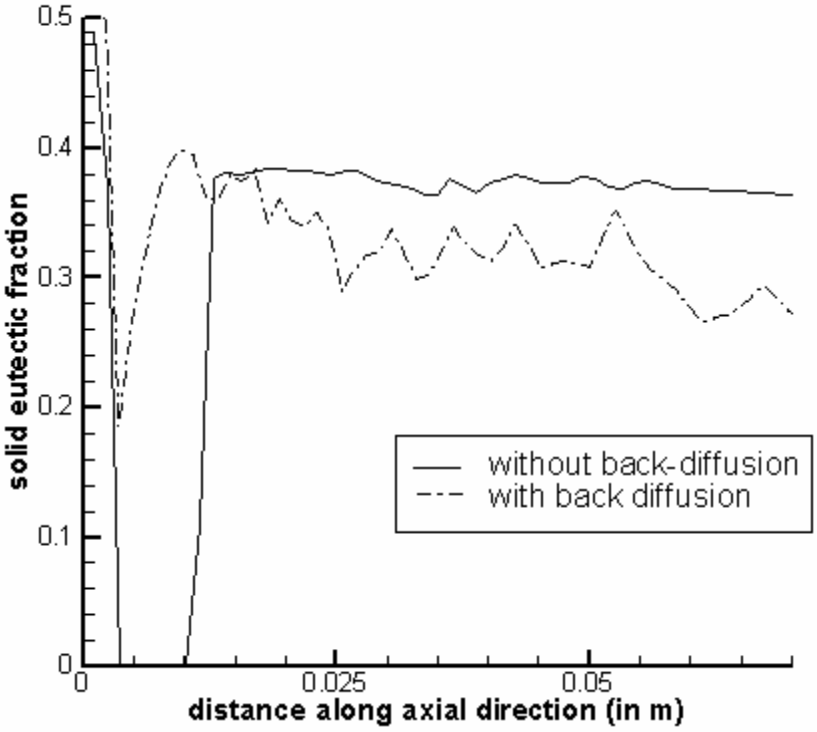

Figure 9 : Effect of back diffusion parameter